Phase diagram of iron pnictides if doping acts as a source of disorder

M. G. Vavilov and A. V. Chubukov
Department of Physics, University of Wisconsin, Madison, Wisconsin 53706, USA
(Received 5 October 2011; revised manuscript received 14 November 2011; published 19 December 2011)

We obtain and analyze the phase diagram of doped iron pnictides under the assumption that doping adds nonmagnetic impurities to the system but does not change the densities of carriers. We show that the phase diagram is quite similar to the one obtained under the opposite rigid band assumption. In both cases, there is a phase where $s^{\pm}$ superconductivity and antiferromagnetism coexist. We evaluate the jump of the specific heat, ΔC, at the superconducting T_c across the phase diagram and show that $\Delta C/T_c$ is nonmonotonic, with the maximum at the onset of the coexistence phase. Our results are in quantitative agreement with experiments on some iron pnictides.

DOI: 10.1103/PhysRevB.84.214521 PACS number(s): 74.70.Xa, 74.25.Bt, 74.62.−c

I. INTRODUCTION

How chemical doping of iron pnictides affects their electronic structure is not fully understood yet and is subject of debates. In most studies, it is assumed that doping does not affect the rigid band picture and only changes the densities of holes and electrons.[1] An alternative scenario[2] is that doping does not affect the carrier density but rather introduces nonmagnetic impurities and hence increases disorder. Angle-resolved photoemission (ARPES) experiments on 122 materials $Ba(Fe_{1-x}Co_x)_2As_2$ and $Ba_{1-x}K_xFe_2As_2$ are usually interpreted in favor of the rigid band scenario. Within this scenario, if magnetism prevails at zero doping, the system moves from a spin-density-wave (SDW) phase to a superconducting (SC) state, and for some model parameters, there is a mixed phase where SDW and SC orders coexist.[3–5] Recent ARPES experiments on Ru-doped $BaFe_2As_2$, however, found[6,7] that substitution of Fe with Ru practically does not change the Fermi surface (FS), yet the phase diagram is quite similar to that in other doped 122 materials; as Ru concentration increases, the system moves from an SDW phase to an SC phase. In between, there is a region where where both SDW and SC orders coexist, although microscopic coexistence (as opposed to phase separation) has not been experimentally proven yet.[8] Because FS geometry does not change, it seems natural to assume that the changes in the phase diagram caused by Ru-substitution are predominantly due to dilution and disorder associated with it. We also note that disorder may be introduced directly to pnictide materials by irradiation.[9,10]

In the present paper, we address the issue of what is the phase diagram of a doped 122 Fe-pnictide if doping does not affect the carrier density but rather introduces nonmagnetic impurities. We show that the phase diagram is actually the same as in the rigid band scenario. Namely, as doping increases, first an SDW phase becomes a mixed phase, then the system becomes a pure $s^{\pm}$ SC, and at even larger dopings, $s^{\pm}$ SC is destroyed by disorder. This result may look somewhat counterintuitive because nonmagnetic impurities are pair breaking for an $s^{\pm}$ SC. It turns out, however, that impurities damage SDW order stronger than they damage $s^{\pm}$ SC because both intra and interband impurity scattering is destructive for SDW,[11] while only interband scattering is pair breaking for an $s^{\pm}$ SC.[12–14] Because of this disparity, the actual magnetic T_s becomes smaller than the superconducting T_c when the density of impurities exceeds a certain threshold, even for the undoped case $T_s > T_c$. There is no *a priori* guarantee that a mixed state emerges near the point where $T_s = T_c$, i.e., a first-order transition from an SDW to a SC is another option. Our calculation shows that the mixed state does appear, see Fig. 1(a). For such a phase diagram to emerge, the magnetic SDW $T_{s,0}$ for an undoped material should not be too strong compared to $T_{c,0}$, see below. If $T_{s,0}/T_{c,0}$ is too large, T_s remains higher than T_c down to $T_c \to 0$, even though T_s decreases faster.

There is another reason to analyze the phase diagram assuming that doping introduces disorder. The measurements of the specific heat jump ΔC at T_c across the phase diagram have demonstrated[15–18] that $\Delta C/T_c$ is nonmonotonic and has a maximum at optimal doping that almost coincides with the onset of the coexistence phase. The slopes of $\Delta C/T_c$ are similar, although not exactly identical, upon deviations from optimal doping into both directions. This similarity raised speculations that the behavior of $\Delta C/T_c$ in underdoped and overdoped regimes may be related. Within the rigid-band model, $\Delta C/T_c$ has a peak at the onset of a mixed phase and rapidly decreases at lower doping.[19] However, the reduction of $\Delta C/T_c$ at higher doping cannot be straightforwardly explained within the rigid-band model.

In the disorder model, the behavior of $\Delta C/T_c$ across the whole phase diagram is determined by a single parameter, the density of impurities n_{imp}, and the forms of $\Delta C/T_c$ in the underdoped and overdoped regimes are related. We find that in the disordered model, $\Delta C/T_c$ indeed decreases on both sides of optimal doping, as shown in Figs. 1(b) and 2. The specific heat is discontinuous at the onset of the mixed phase within the mean-field approximation, but becomes rounded once fluctuations are taken into account. The decrease of $\Delta C/T_c$ away from the maximum shows rather similar, although not identical, behavior in under and overdoped regimes, with roughly quadratic dependence on the transition temperature T_c, see Fig. 2(b). This behavior is in quantitative agreement with experiments.[15–17]

The fact that the phase diagram and the behavior of $\Delta C/T_c$ are similar in the rigid-band and the disorder models is encouraging, since the two models are complementary to

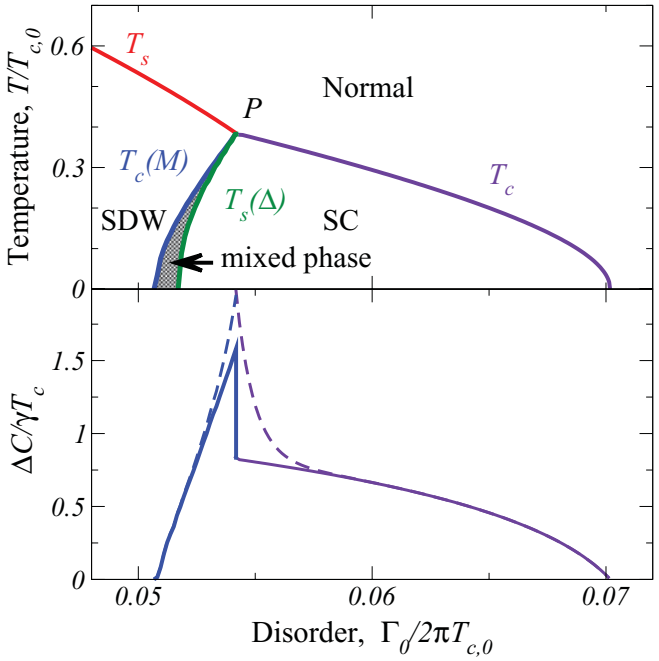

FIG. 1. (Color online) (Upper panel) The phase diagram as a function of disorder, measured in units $\Gamma_0/2\pi T_{c,0} \propto n_{\rm imp}$, for on-site disorder ($\Gamma_\pi = \Gamma_0$) and $T_{s,0}/T_{c,0} = 1.7$. The four transition lines terminate at a tetracritical point P, where normal, pure SDW, pure SC, and mixed phases meet. The shaded region represents the mixed phase. (Lower panel) Specific heat jump $\Delta C/T_c$ as a function of doping. Solid curves represent the mean-field result and the dashed curve illustrates the effect of thermodynamic fluctuations beyond the mean-field theory.

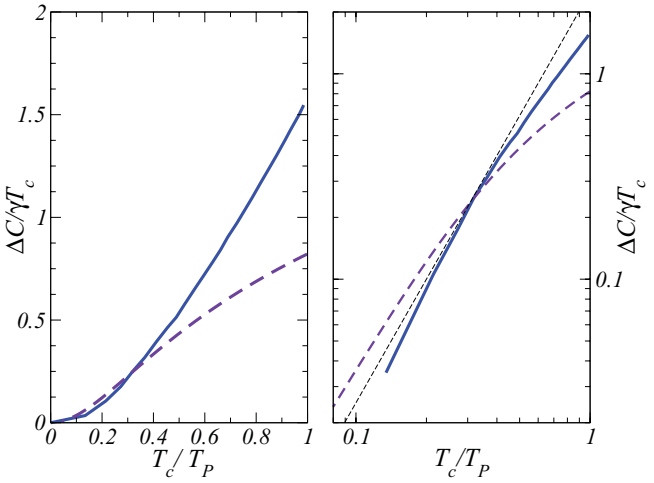

FIG. 2. (Color online) The specific heat jump $\Delta C/T_c$ for $\Gamma_\pi = \Gamma_0$ and $T_{s,0} = 1.7T_{c,0}$, as a function of T_c/T_P, where T_P is the temperature of the tetracritical point. Left panel: linear scale, right panel: log-log scale. The solid line represents the specific heat jump $\Delta C/T_c$ at $T_c(M)$ in the mixed phase in the underdoped regime, and the dashed line represents $\Delta C/T_c$ in the overdoped regime, where SDW order is absent. A thin dash line represents a quadratic dependence $\Delta C/T_c \propto T_c^2$.

each other. In general, a chemical doping acts in both ways: (1) doping introduces some extra carriers and (2) increases impurity density. The relative magnitude of the two effects depends on materials. We argue in this regard that quite similar behavior observed in Ru-, Co-, and K-doped $BaFe_2As_2$[15–18] is not a coincidence but rather a quite generic feature of iron pnictides.

The paper is organized as follows. In the next section, we discuss the model and introduce SDW and SC order parameters and describe the formalism used for calculations. In Sec. III, we analyze the phase diagram as a function of impurity concentration, by solving a linearized gap equation for one order parameter, SDW or SC, when the second parameter is either absent or present. Section IV presents calculations of the superconducting order parameter near the transition to a superconducting state. In Sec. V, we consider specific heat jump at the onset of superconductivity. We provide our conclusions in Sec. VI.

II. THE MODEL

A. General formulation

Our goal is to demonstrate that the phase diagram remains the same if we associate doping with disorder rather than with the changes to the FS in the rigid-band picture. We adopt the same minimal model that was used in earlier works within the rigid-band approach.[19] Namely, we consider a two-band metal with cylindrical FSs for electron and hole-type excitations. The cylindrical FSs have circular cross sections of equal radii centered at (0,0) with a holelike dispersion and $\boldsymbol{Q} = (0,\pi)$ with an electron-like dispersion. The free fermion part of the Hamiltonian in this case of perfect nesting is represented by

$$\mathcal{H}_0 = -\sum_{\boldsymbol{p},\alpha} \xi(\boldsymbol{p}) \hat{c}^\dagger_{\boldsymbol{p}\alpha} \hat{c}_{\boldsymbol{p}\alpha} + \sum_{\boldsymbol{p},\alpha} \xi(\tilde{\boldsymbol{p}}) \hat{f}^\dagger_{\tilde{\boldsymbol{p}}\alpha} \hat{f}_{\tilde{\boldsymbol{p}}\alpha},$$

where operators $\hat{c}$ annihilate holelike fermions near (0,0) and operators $\hat{f}$ annihilate electron-like fermions near $\boldsymbol{Q}$. The fermionic dispersion is given by $\xi(\boldsymbol{p}) = \boldsymbol{p}^2/2m - \mu$, and the momentum $\tilde{\boldsymbol{p}}$ of electron excitations is measured as a deviation from $\boldsymbol{Q}$, $\tilde{\boldsymbol{p}} = \boldsymbol{p} - \boldsymbol{Q}$.

We consider an effective low-energy theory with the high-energy cutoff Λ and angle-independent interactions in the SDW channel and in the $s^\pm$ SC channel with the couplings $\lambda_{\rm sdw}$ and $\lambda_{\rm sc}$.[4,20–24] We treat these interactions within a mean-field approximation, by introducing SC and SDW order parameters, Δ and $\mathbf{M}$, respectively, and decomposing the four-fermion interactions into effective quadratic terms with Δ and $\mathbf{M}$ in the prefactors. The full mean-field Hamiltonian is quadratic in fermionic operators and can be written as

$$\mathcal{H} = \frac{1}{2} \sum_{\boldsymbol{p},\alpha,\beta} \overline{\Psi}_{\boldsymbol{p},\alpha} \hat{H}_{\boldsymbol{p},\alpha,\beta} \Psi_{\boldsymbol{p},\beta}, \qquad (1)$$

where $\overline{\Psi}_{\boldsymbol{p},\alpha} = (\hat{c}^\dagger_{\boldsymbol{p},\alpha},\ \hat{c}_{-\boldsymbol{p},\alpha},\ \hat{f}^\dagger_{\boldsymbol{p},\alpha},\ \hat{f}_{-\boldsymbol{p},\alpha})$ and $\Psi_{\boldsymbol{p},\alpha}$ is a conjugated column. The Hamiltonian matrix $\hat{H}_{\boldsymbol{p},\alpha,\beta}$ can be written in the form[4]

$$\begin{aligned} \hat{H} &= \hat{H}_0 + \hat{H}_{\rm mf}, \quad \hat{H}_0 = -\xi \hat{\tau}_3 \hat{\rho}_3 \hat{\sigma}_0, \\ \hat{H}_{\rm mf} &= -\Delta \hat{\tau}_2 \hat{\rho}_3 \hat{\sigma}_2 + \hat{\tau}_3 \hat{\rho}_1 (\boldsymbol{M}\hat{\boldsymbol{\sigma}}). \end{aligned} \qquad (2)$$

Here, the Pauli matrices $\hat{\tau}_i$, $\hat{\rho}_i$ and $\hat{\sigma}_i$ are defined in the Gorkov-Nambu, band, and spin spaces, respectively, with $i = 0,1,2,3$

and matrices, where $i = 0$ are unit matrices. A fermion Green's function $\hat{G}(\omega_n, \boldsymbol{p})$ is defined as a solution to

$$(i\omega_n - \hat{H}_{\boldsymbol{p}} - \hat{\Sigma})\hat{G}(\omega_n, \boldsymbol{p}) = \hat{1}, \tag{3a}$$

and the conjugated equation is

$$\hat{G}(\omega_n, \boldsymbol{p})(i\omega_n - \hat{H}_{\boldsymbol{p}} - \hat{\Sigma}) = \hat{1}. \tag{3b}$$

Here, $\hat{\Sigma}$ is the self-energy for scattering off disorder and $\omega_n = 2\pi T_m(n + 1/2)$ with integer n are Matsubara frequencies.

We describe disorder scattering within the Born approximation and assume that the Born scattering amplitude $U(\boldsymbol{q})$ is characterized by a constant U_0 for scattering within the same band and U_π for scattering between the two bands.[12–14] In this approximation, the self-energy is

$$\hat{\Sigma}(\omega_n) = \frac{4\Gamma_0}{\pi N_F}\int \frac{d\boldsymbol{p}}{(2\pi\hbar)^2}\hat{\tau}_3\hat{\rho}_0\hat{\sigma}_0\hat{G}(\omega_n,\xi)\hat{\tau}_3\hat{\rho}_0\hat{\sigma}_0 + \frac{4\Gamma_\pi}{\pi N_F}\int \frac{d\boldsymbol{p}}{(2\pi\hbar)^2}\hat{\tau}_3\hat{\rho}_1\hat{\sigma}_0\hat{G}(\omega_n,\xi)\hat{\tau}_3\hat{\rho}_1\hat{\sigma}_0, \tag{4}$$

where we introduced disorder scattering rates:

$$\Gamma_0 = \frac{\pi N_F n_{\rm imp}}{4}|U_0|^2, \quad \Gamma_\pi = \frac{\pi N_F n_{\rm imp}}{4}|U_\pi|^2. \tag{5}$$

Γ_0 characterizes the rate of electron collisions with impurities in which the electron remains in its original band, while Γ_π is the rate of collisions resulting in electron transfer between the two bands. N_F in Eq. (5) is the total quasiparticle density of states (DoS) at the Fermi energy (the DoS per spin per band is $N_F/4$). We assume that only the impurity density $n_{\rm imp}$ changes with doping, i.e., the ratio Γ_π/Γ_0 is doping independent.

The two mean-field parameters Δ and $\mathbf{M}$ are obtained self-consistently via the matrix Green's function as

$$\frac{\Delta}{\lambda_{\rm sc}} = \frac{T}{2}\sum_{\omega_n}\int \frac{d\boldsymbol{p}}{(2\pi\hbar)^2}{\rm Tr}[\hat{G}(\omega_n,\boldsymbol{p})\hat{\tau}^+(\hat{\rho}_0 + \hat{\rho}_3)\hat{\sigma}^+], \tag{6}$$

and

$$\frac{\boldsymbol{M}}{\lambda_{\rm sdw}} = \frac{T}{4}\sum_{\omega_n}\int\int \frac{d\boldsymbol{p}}{(2\pi\hbar)^2}{\rm Tr}[\hat{G}(\omega_n,\boldsymbol{p})(\hat{\tau}_0 + \hat{\tau}_3)\hat{\rho}^+\hat{\boldsymbol{\sigma}}], \tag{7}$$

where $\hat{A}^+ = (\hat{A}_1 + i\hat{A}_2)/2$ for $\hat{A} \to \hat{\rho}, \hat{\tau}, \hat{\sigma}$.

For the pure SDW and the pure s^{+-} SC state in the absence of disorder, the solution of the linearized gap equations yields transition temperatures $T_{s,0} = 1.13\Lambda\exp[-2/(N_F\lambda_{\rm sdw})]$ and $T_{c,0} = 1.13\Lambda\exp[-2/(N_F\lambda_{\rm sc})]$. We consider $T_{s,0} > T_{c,0}$, so that without disorder, the SDW phase develops at a higher temperature.

B. Eilenberger equation

To treat superconductivity and magnetism in the presence of disorder, it is convenient to introduce the Eilenberger's Green function

$$\hat{\mathcal{G}}(\omega_n) = \frac{4i}{\pi N_F}\int \frac{d\boldsymbol{p}}{(2\pi\hbar)^2}\hat{\tau}_3\hat{\rho}_3\hat{\sigma}_0\hat{G}(\omega_n,\boldsymbol{p}), \tag{8}$$

which appears both in the self-consistency equations, Eqs. (6) and (7), and in the expression for the impurity self-energy, Eq. (4). In particular, the impurity self-energy is

$$\hat{\Sigma} = -i\Gamma_0\hat{\tau}_0\hat{\rho}_3\hat{\sigma}_0\hat{\mathcal{G}}\hat{\tau}_3\hat{\rho}_0\hat{\sigma}_0 - i\Gamma_\pi\hat{\tau}_0(-i\hat{\rho}_2)\hat{\sigma}_0\hat{\mathcal{G}}\hat{\tau}_3\hat{\rho}_1\hat{\sigma}_0. \tag{9}$$

To derive the equation for $\hat{\mathcal{G}}$, we multiply Eq. (3a) by $\hat{\tau}_3\hat{\rho}_3$ from left and subtract Eq. (3b), multiplied by $\hat{\tau}_3\hat{\rho}_3$ from right. We then multiply the resulting equation by $\hat{\tau}_3\hat{\rho}_3$ from left again. As a result, the $\hat{H}_0(\boldsymbol{p})$ term falls out. We integrate the resulting equation over $\boldsymbol{p}$ and obtain the equation for $\hat{\mathcal{G}}(\omega_n)$ in the form of a commutator:

$$[i\omega_n\hat{\tau}_3\hat{\rho}_3\hat{\sigma}_0 - (\hat{H}_{\rm mf} + \hat{\Sigma})\hat{\tau}_3\hat{\rho}_3\hat{\sigma}_0; \hat{\mathcal{G}}(\omega_n)] = 0. \tag{10}$$

This equation is the Eilenberger equation,[25,26] obtained for a two-band metal with homogeneous in space SDW and SC order parameters. The Eilenberger equation is consistent with the normalization relations for $\hat{\mathcal{G}}$: ${\rm Tr}\hat{\mathcal{G}}(\omega_n) = 0$ and $\hat{\mathcal{G}}(\omega_n)\hat{\mathcal{G}}(\omega_n) = \hat{1}$.

Without loss of generality, we direct $\boldsymbol{M}$ along z axis and parametrize the matrix $\hat{\mathcal{G}}(\omega_n)$ by the three functions g_{ω_n}, f_{ω_n}, and S_{ω_n} as

$$\hat{\mathcal{G}}(\omega_n) = g_{\omega_n}\hat{\tau}_3\hat{\rho}_3\hat{\sigma}_0 + f_{\omega_n}\hat{\tau}_1\hat{\rho}_0(-i\hat{\sigma}_2) + S_{\omega_n}\hat{\tau}_0(-i\hat{\rho}_2)\hat{\sigma}_3. \tag{11}$$

The function g_{ω_n} is the normal component of the Eilenberger Green's function, while the functions S_{ω_n} and f_{ω_n} are the two anomalous components, associated with the SDW and SC orders, respectively.

For the above parametrization of $\hat{\mathcal{G}}(\omega_n)$, Eq. (11), the normalization condition $\hat{\mathcal{G}}\hat{\mathcal{G}} = 1$ reduces to

$$g_{\omega_n}^2 - S_{\omega_n}^2 - f_{\omega_n}^2 = 1, \tag{12}$$

and the commutation relation, Eq. (10), gives

$$i\Delta g_{\omega_n} = f_{\omega_n}(\omega_n + 2\Gamma_\pi g_{\omega_n}), \tag{13a}$$

$$iMg_{\omega_n} = S_{\omega_n}(\omega_n + 2\Gamma_t g_{\omega_n}), \tag{13b}$$

where $\Gamma_t = \Gamma_0 + \Gamma_\pi$.

The self-consistency equations for SDW and SC order parameters, Eqs. (6) and (7), can be rewritten in terms of anomalous SDW and SC components of the Eilenberger's Green function as

$$\frac{2M}{N_F\lambda_{\rm sdw}} = -i2\pi T\sum_{\omega_n>0}^{\Lambda} S_{\omega_n}, \tag{14a}$$

$$\frac{2\Delta}{N_F\lambda_{\rm sc}} = -i2\pi T\sum_{\omega_n>0}^{\Lambda} f_{\omega_n}. \tag{14b}$$

III. PHASE DIAGRAM

We first consider pure SDW and SC states. For a pure SDW state, we set $\Delta = 0$ and $f_{\omega_n} = 0$ in Eqs. (12) and (13a), linearize Eq. (13b) in M and find from Eq. (14a) that the SDW transition temperature T_s evolves with doping as

$$\frac{2}{N_F\lambda_{\rm sdw}} = 2\pi T_s\sum_{n\geqslant 0}^{\Lambda/2\pi T_s}\frac{1}{\pi T_s(2n+1) + 2\Gamma_t}. \tag{15}$$

This equation can be rewritten in terms of the transition temperature $T_{s,0}$ to SDW phase at $\Gamma_t = 0$ as

$$\ln\frac{T_{s,0}}{T_s} = \psi\left(\frac{1}{2} + \frac{\Gamma_t}{\pi T_s}\right) - \psi\left(\frac{1}{2}\right), \tag{16}$$

where $\psi(x)$ is the digamma function.[11]

For a pure SC state, we set $M = 0$ and $S_{\omega_n} = 0$ in Eqs. (12) and (13b) and linearize Eq. (13a) in Δ. We obtain from Eq. (14b),

$$\frac{2}{N_F \lambda_{\rm sc}} = 2\pi T_c \sum_{n\geqslant 0}^{\Lambda/2\pi T_c} \frac{1}{\pi T_c(2n+1) + 2\Gamma_\pi}. \tag{17}$$

Reexpressing the result in terms of the superconducting transition temperature $T_{c,0}$ in a clean system and without SDW, we rewrite Eq. (17) as

$$\ln \frac{T_{c,0}}{T_c} = \psi\left(\frac{1}{2} + \frac{\Gamma_\pi}{\pi T_c}\right) - \psi\left(\frac{1}{2}\right), \tag{18}$$

which is similar to the equation for T_c in conventional s-wave superconductors with magnetic impurities[27] and in unconventional d-wave superconductors with potential impurities.[28–30] Note that only interband scattering Γ_π, is pair breaking for $s^\pm$ SC.

Even if $T_{s,0} > T_{c,0}$, T_s decreases faster than T_c with increasing $n_{\rm imp}$, and at certain doping, the two transition temperatures may cross. We denote this temperature as T_P. The condition that T_P exists, i.e., that T_c and T_s cross before $T_c \to 0$, sets the limits on the ratios $T_{s,0}/T_{c,0}$ and Γ_π/Γ_0. We find that T_s and T_c cross if $T_{c,0}/T_{s,0} > 1/(1+\Gamma_0/\Gamma_\pi)$. For an on-site disorder potential $\Gamma_\pi = \Gamma_0$, $T_P > 0$ exists, i.e., SC phase exists, if $T_{c,0}/T_{s,0} > 1/2$. For longer-range impurity potentials, $\Gamma_0 > \Gamma_\pi$, the SC phase develops even for smaller $T_{c,0}/T_{s,0}$, see Figs. 1(a) and 3(a).

To obtain the superconducting transition temperature $T_c(M)$ in the presence of pre-existing magnetism, one has to solve the linearized equation for Δ at a finite M. Now g_{ω_n} depends on M [i.e., $g_{\omega_n} = g_{\omega_n}(M)$], and we have from Eq. (14b),

$$\alpha(T_c(M)) = \frac{2}{N_F \lambda_{\rm sc}}, \tag{19}$$

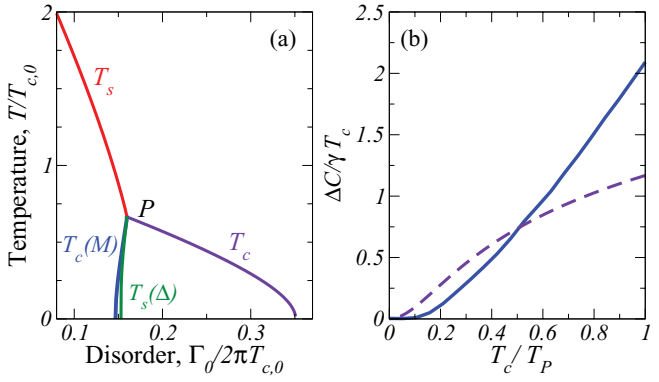

FIG. 3. (Color online) (a) The phase diagram as a function of disorder, $\Gamma_0/2\pi T_{c,0}$ for $\Gamma_\pi = 0.2\Gamma_0$ and $T_{s,0}/T_{c,0} = 3$. Note that the region of the mixed phases gets narrower than the region for on-site impurities, c.f. 1. (b) The specific heat jump as a function of T_c/T_P. The solid line represents the specific heat jump $\Delta C/T_c$ for normal-to-SC transition, and the dashed line shows $\Delta C/T_c$ in the overdoped region for transition between SDW and SC coexistence phases.

where

$$\alpha(T) = 2\pi T \sum_{\omega_n>0}^{\Lambda} \frac{g_{\omega_n}(M)}{\omega_n + 2\Gamma_\pi g_{\omega_n}(M)}. \tag{20}$$

The temperature dependence in the right-hand side of Eq. (20) is via $\omega_n = \pi T(2n+1)$ and also via $g_{\omega_n}(M)$ because M depends on temperature. The summation in $\alpha(T)$ has a logarithmic dependence on the high-energy cutoff Λ. This dependence can be eliminated in favor of the transition temperature T_c at $M = 0$. Subtracting Eq. (17) from Eq. (19), we obtain after a simple algebra an equation on $T_c(M)$ in the form

$$\mathcal{L}[T_c(M), T_c, \Gamma_\pi] = \sum_{\omega_n>0}^{\Lambda} \frac{2\pi T_c(M)\omega_n\big[g_{\omega_n}(M) - 1\big]}{(\omega_n + 2\Gamma_\pi)\big[\omega_n + 2\Gamma_\pi g_{\omega_n}(M)\big]}, \tag{21}$$

where

$$\mathcal{L}(T_1, T_2, \Gamma) = \ln \frac{T_1}{T_2} + \psi\left(\frac{1}{2} + \frac{\Gamma}{\pi T_1}\right) - \psi\left(\frac{1}{2} + \frac{\Gamma}{\pi T_2}\right). \tag{22}$$

We calculate $g_{\omega_n}(M)$ as a function of temperature at a given impurity concentration. For this purpose, we express $S_{\omega_n}(M)$ in terms of $g_{\omega_n}(M)$ using Eq. (13b),

$$S_{\omega_n}(M) = \frac{iMg_{\omega_n}(M)}{\omega_n + 2\Gamma_t g_{\omega_n}(M)}, \tag{23}$$

substitute the result into Eq. (12) with $f_{\omega_n} = 0$, and obtain the fourth-order algebraic equation for $g_{\omega_n}(M)$ as a function of M:

$$g^2_{\omega_n}(M) + \frac{M^2 g^2_{\omega_n}(M)}{\big[\omega_n + 2\Gamma_t g_{\omega_n}(M)\big]^2} = 1. \tag{24}$$

We solve this equation, obtain $g_{\omega_n}(M)$, substitute the result back into Eqs. (23) and (14a), utilize the definition of T_s, and obtain the nonlinear equation for $M = M(T)$ in the form

$$\mathcal{L}(T, T_s, \Gamma_t) = 2\pi T \sum_{\omega_n>0} \frac{\omega_n\big[g_{\omega_n}(M) - 1\big]}{(\omega_n + 2\Gamma_t)\big[\omega_n + 2\Gamma_t g_{\omega_n}(M)\big]}, \tag{25}$$

where $g_{\omega_n}(M)$ is a solution of Eq. (24), one has to choose the branch with $g_{\omega_n}(M=0) = 1$. Solving Eq. (25) we obtain $M(T)$, and hence $g_{\omega_n}(T)$. Substituting the result into Eqs. (19) and (20) we obtain the superconducting transition temperature $T_c(M)$ in the mixed phase as a function of doping.

We numerically evaluate $T_c(M)$ at different dopings in the mixed phase and plot the result in Figs. 1(a) and 3(a). As the doping decreases from its optimal value, M increases at a given temperature T, and $T_c(M)$ rapidly drops. This is expected since SDW and SC order parameters compete with each other. At $M \to 0$, $g_{\omega_n}(M) \to 1$, and Eq. (21) yields $T_c(M) \to T_c$, as expected.

A similar calculation of the SDW transition temperature from the preexisting SC phase, $T_s(\Delta)$, shows that $T_s(\Delta)$ decreases as Δ increases due to the same kind of competition. Furthermore, the $T_s(\Delta)$ curve actually bends toward smaller dopings, see Figs. 1(a) and 3(a), so that with decreasing temperature the system moves from a pure SDW magnet to

a pure superconductor through a mixed phase. The bending of the $T_s(\Delta)$ curve is in agreement with the general analysis in Ref. 31. The four curves T_c, $T_c(M)$, T_s, and $T_s(\Delta)$ meet at the tetracritical point P, as shown in Figs. 1(a) and 3(a). The corresponding temperature T_P is the highest superconducting transition temperature. We also see from numerics that, despite bending, the curve $T_s(\Delta)$ is always located to the right of the curve $T_c(M)$, i.e., if one increases disorder at a given T or decreases T at a given disorder, the system with the SDW order first becomes unstable toward an intermediate mixed phase where SDW and SC orders coexist, and only then SDW order disappears.

The intermediate mixed phase was earlier found in the rigid-band model.[3,4] However, in that model, it only appears at a finite ellipticity of electron pockets, while for circular hole and electron FSs, doping gives rise to a first-order transition between pure SDW and pure SC phases. In the disorder model, the mixed phase appears already for circular hole and electron pockets and by continuity should also exists when electron pockets have weak ellipticity. We, however, did not analyze the whole range of ellipticities and therefore cannot exclude a possibility of a first-order transition for strongly elliptical electron FSs.

IV. SUPERCONDUCTING ORDER PARAMETER NEAR T_c

We verified that the mixed phase does indeed exist in the disorder model with circular FSs by expanding in Eq. (13a) to order Δ^3 and solving the equation for Δ in the presence of $\boldsymbol{M}$ at a temperature slightly below $T_c(M)$. The expansion yields, quite generally,

$$\alpha(T) - \beta\Delta^2 = \frac{2}{\lambda_{\rm sc} N_F}, \tag{26}$$

where $\alpha(T)$ is introduced in Eq. (20) and $\beta = \beta(T_c(M))$ is given by Eq. (37) below. Near $T_c(M)$, we have $\alpha(T) = \alpha[T_c(M)] + \alpha'[T_c(M)][T - T_c(M)]$ and $\alpha[T_c(M)]$, see Eq. (19). On general grounds, $\alpha'[T_c(M)]$ must be negative for a SC phase to develop as T decreases, and we indeed show below that $\alpha'[T_c(M)] < 0$. The type of the transition is, however, determined by the sign of β. The mixed phase exists if $\beta > 0$ because then Δ gradually grows as T decreases. If $\beta < 0$, Δ changes discontinuously around $T_c(M)$ and the SDW and SC phases are separated by the first-order transition.[3,4]

The coefficient $\alpha(T)$ can be rewritten in the form of Eqs. (21) and (22):

$$\alpha(T) = \frac{2}{\lambda_{\rm sc} N_F} - Y(T), \quad \alpha'(T) = -\frac{\partial Y(T)}{\partial T}, \tag{27}$$

where

$$Y(T) = \mathcal{L}(T, T_c, \Gamma_\pi) + \sum_{\omega_n > 0} \frac{2\pi T \omega_n \left[1 - g_{\omega_n}(M)\right]}{[\omega_n + 2\Gamma_\pi]\left[\omega_n + 2\Gamma_\pi g_{\omega_n}(M)\right]}. \tag{28}$$

For $M = 0$ and in the clean limit, $\alpha'(T_c) = -1/T_c$. We verified numerically that $\alpha'[T_c(M)]$ remains negative at $M \neq 0$ and in the presence of disorder, as expected.

Calculations of β require more care as one has to combine terms coming from the appearance of nonzero f_{ω_n} in Eq. (12) and from the expansion of the SDW order parameter $M(\Delta)$ to order Δ^2 as $M(\Delta) = M + \delta M^{(2)}$, where $\delta M^{(2)} \propto \Delta^2$. Similarly, we introduce $g_{\omega_n} = g_{\omega_n}(M) + \delta g^{(2)}_{\omega_n}$ and $S_{\omega_n} = S_{\omega_n}(M) + \delta S^{(2)}_{\omega_n}$. Substituting g_{ω_n} and S_{ω_n} into Eqs. (12) and (13b), we obtain equations for $\delta g^{(2)}_{\omega_n}$ and $\delta S^{(2)}_{\omega_n}$,

$$\begin{aligned} g_{\omega_n}(M)\delta g^{(2)}_{\omega_n} - S_{\omega_n}(M)\delta S^{(2)}_{\omega_n} &= \tfrac{1}{2}\left[f^{(1)}_{\omega_n}\right]^2, \\ \frac{-iM\omega_n \delta g^{(2)}_{\omega_n}}{\left[\omega_n + 2\Gamma_t g_{\omega_n}(M)\right]^2} + \delta S^{(2)}_{\omega_n} &= \frac{i\delta M^{(2)} g_{\omega_n}(M)}{\omega_n + 2\Gamma_t g_{\omega_n}(M)}, \end{aligned} \tag{29}$$

where

$$f^{(1)}_{\omega_n} = \frac{i\Delta g_{\omega_n}(M)}{\omega_n + 2\Gamma_\pi g_{\omega_n}(M)}, \tag{30}$$

and $g_{\omega_n}(M)$ is defined by Eq. (23). Solving Eq. (29), we obtain

$$\delta g^{(2)}_{\omega_n} = -\frac{1}{2}\frac{g_{\omega_n}(M)\left[\omega_n + 2\Gamma_t g_{\omega_n}(M)\right]^2}{\left[\omega_n + 2\Gamma_t g_{\omega_n}(M)\right]^3 + M^2\omega_n} \times \left\{\Delta^2 \frac{\omega_n + 2\Gamma_t g_{\omega_n}(M)}{\left[\omega_n + 2\Gamma_\pi g_{\omega_n}(M)\right]^2} + \frac{2M\delta M^{(2)}}{\omega_n + 2\Gamma_t g_{\omega_n}(M)}\right\} \tag{31}$$

and

$$\delta S^{(2)}_{\omega_n} = -\frac{i}{2}\frac{g_{\omega_n}(M)\left(\omega_n + 2\Gamma_t g_{\omega_n}(M)\right)^2}{\left[\omega_n + 2\Gamma_t g_{\omega_n}(M)\right]^3 + M^2\omega_n} \times \left\{\frac{\Delta^2 M\omega_n}{\left[\omega_n + 2\Gamma_\pi g_{\omega_n}(M)\right]^2\left[\omega_n + 2\Gamma_t g_{\omega_n}(M)\right]} - 2\delta M^{(2)}\right\}. \tag{32}$$

We first evaluate $\delta M^{(2)}$ by substituting $S_{\omega_n} = S^{(0)}_{\omega_n} + S^{(2)}_{\omega_n}$ into Eq. (14a) and eliminating the SDW coupling constant in favor of the SDW transition temperature T_s, see Eq. (15). We obtain

$$\delta M^{(2)} \mathcal{L}(T, T_s, \Gamma_t) = -2\pi T \sum_{\omega_n > 0}\left(i\delta S^{(2)}_{\omega_n} + \frac{\delta M^{(2)}}{\omega_n + 2\Gamma_t}\right). \tag{33}$$

Substituting $\mathcal{L}(T, T_s, \Gamma_t) \approx \mathcal{L}[T_c(M), T_s, \Gamma_t]$ from Eq. (25) and $\delta S^{(2)}_{\omega_n}$ from Eq. (32), we obtain

$$\delta M^{(2)} = -\frac{\Delta^2}{2M}\frac{C}{B}, \tag{34}$$

where the coefficients B and C, together with the term A, which we utilize below, are given by

$$A = \pi T \sum_{\omega_n > 0} \frac{g_{\omega_n}(M)\omega_n\left[\omega_n + 2\Gamma_t g_{\omega_n}(M)\right]^3}{\left[\omega_n + 2\Gamma_\pi g_{\omega_n}(M)\right]^4 D}, \tag{35a}$$

$$B = \pi T \sum_{\omega_n > 0} \frac{g_{\omega_n}(M)\omega_n}{\left[\omega_n + 2\Gamma_t g_{\omega_n}(M)\right] D}, \tag{35b}$$

$$C = \pi T \sum_{\omega_n > 0} \frac{g_{\omega_n}(M)\omega_n\left[\omega_n + 2\Gamma_t g_{\omega_n}(M)\right]}{\left[\omega_n + 2\Gamma_\pi g_{\omega_n}(M)\right]^2 D}, \tag{35c}$$

$$D = \left[\omega_n + 2\Gamma_t g_{\omega_n}(M)\right]^3 + \omega_n M^2. \tag{35d}$$

Substituting $\delta M^{(2)}$ into Eq. (31), we obtain $\delta g^{(2)} \propto \Delta^2$.

We next write f_{ω_n}, defined by Eq. (13a) to the third order in Δ:

$$f_{\omega_m} = \frac{i\Delta g_{\omega_n}(M)}{\omega_n + 2\Gamma_\pi g_{\omega_n}(M)} + \frac{i\Delta\omega_n g^{(2)}_{\omega_n}}{\left[\omega_n + 2\Gamma_\pi g_{\omega_n}(M)\right]^2}, \quad (36)$$

substitute this expression into Eq. (14b), and obtain Eq. (26) with

$$\beta = \left(A - \frac{C^2}{B}\right), \quad (37)$$

where A, B, and C are given by Eq. (35).

Evaluating these coefficients, we find $AB > C^2$, i.e., β is positive. This confirms our numerical result that the phase diagram of the disorder model contains the mixed phase where SDW and SC orders coexist.

Equation (26) can also be applied to the transition from a paramagnetic metal into a pure SC state. In this case, $M = 0$, and hence $g_{\omega_n} = g_{\omega_n}(M) = 1$ and C^2/B term in Eq. (37) is absent, i.e., $\beta = A$. Substituting $g_{\omega_n}(M) = 1$ into Eqs. (35a) and (35d), we obtain

$$\alpha'(T_c) = -\frac{1}{T_c}\left[1 - \sum_{m=0}^{\infty} \frac{\Gamma_\pi/\pi T_c}{(m + 1/2 + \Gamma_\pi/\pi T_c)^2}\right], \quad (38a)$$

$$\beta = \frac{1}{8\pi^2 T_c^2} \sum_{m=0}^{\infty} \frac{m + 1/2}{(m + 1/2 + \Gamma_\pi/\pi T_c)^4}, \quad (38b)$$

where T_c is given by Eq. (18). Note that, again, $\alpha'(T_c) < 0$ and $\beta > 0$.

V. SPECIFIC HEAT JUMP AT THE ONSET OF SUPERCONDUCTIVITY

The specific heat jump at T_c and $T_c(M)$ can be obtained by evaluating the change in the thermodynamic potential $\delta\Omega$ imposed by superconductivity:[32]

$$\Delta\Omega = \int_0^{\Delta} \frac{d\lambda_{sc}^{-1}}{d\Delta_1}\Delta_1^2 d\Delta_1 = -\frac{N_F\beta\Delta^4}{4}, \quad (39)$$

where $d\lambda_{sc}^{-1}/d\Delta$ and Δ^2 are defined by Eq. (26). For Δ^2, we have

$$\Delta^2 = \frac{1}{\beta}\left[\alpha(T) - \frac{2}{\lambda_{sc} N_F}\right] = \frac{|\alpha'|}{\beta}[T_c(M) - T]. \quad (40)$$

The change of the specific heat due to the superconducting ordering is $\Delta C = -T\partial^2\delta\Omega/\partial T^2$. At $T = T_c(M)$, the specific heat exhibits the jump given by

$$\frac{\Delta C}{T_c} = \frac{3\gamma}{2\pi^2}\frac{\{\alpha'[T_c(M)]\}^2}{\beta}, \quad (41)$$

where $\gamma = \pi^2 N_F/3$ is the Sommerfeld coefficient in the metallic phase.

The behavior of $\Delta C/T_c$ as a function of doping-induced disorder is shown in Figs. 1(b), 2, and 3(b). To evaluate $\Delta C/T_c$ at the transition from a normal metal to a superconductor above optimal doping, we use Eq. (38) for α' and β in Eq. (41). At large doping, when T_c is significantly suppressed and the system enters the regime of impurity-induced gapless superconductivity, specific heat jump $\Delta C/T_c$ decreases with

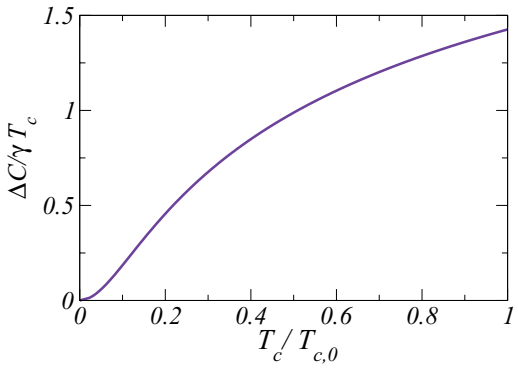

FIG. 4. (Color online) The jump $\Delta C/T_c$ of the specific heat at a superconducting T_c without a competing SDW instability ($\lambda_{sdw} = 0$). $\Delta C/T_c$ is plotted as a function of $T_c/T_{c,0}$, where $T_{c,0}$ is the superconducting transition temperature in the clean limit.

T_c as $\Delta C/T_c \propto T_c^2$, see Ref. 33. Away from the gapless regime, the dependence of $\Delta C/T_c$ on T_c is more complex and differs from T_c^2, as the dashed lines in Figs. 1(b), 2, and 3(b). For completeness, we present in Fig. 4, $\Delta C/T_c$ as a function of $T_c/T_{c,0}$ for an $s^{\pm}$ superconductor, when there is no competing SDW instability (i.e., when $\lambda_{sdw} = 0$) and the T_c line extends to $T_{c,0}$ in the clean limit.

For the transition from the preexisting SDW state into the mixed state below optimal doping, we compute $\Delta C/T_c$, see Eq. (41), using α' and β from Eqs. (27) and (37). In this regime, SDW order strengthens as doping decreases, and SDW correlations suppress both superconducting $T_c(M)$ and $\Delta C/T_c$. In particular, the rapid decrease of $\Delta C/T_c$ at smaller dopings is an indicator that fewer quasiparticle states participate in superconducting pairing, as the low-energy states are pushed away from the FS by SDW order. We see therefore that $\Delta C/T_c$ drops at deviations from optimal doping in both overdopped and underdopped regimes.

It is essential that in the disorder model, the behavior of $\Delta C/T_c$ in the underdoped and overdoped regimes is governed by the single parameter $\Gamma_0 \propto n_{imp}$, assuming that the ratio Γ_π/Γ_0 is kept constant.

The same parameter Γ_0 also defines T_c/T_P, where $T_P = T_c(M \to 0)$ is the transition temperature at the tetracritical point. One can therefore make a direct comparison with experiments by plotting $\Delta C/T_c$ above and below optimal doping as the function of the same T_c/T_P using ΔC defined by Eq. (41) with α' and β given by Eq. (38) above optimal doping, and by Eqs. (27) and (37) for a finite M below optimal doping. Experiments show[15–17] that $\Delta C/T_c$ drops faster in underdoped regime, but in log-log plot the data from underdoped and overdoped regimes can be reasonably well fitted by a quadratic law $\Delta C/T_c \propto T_c^2$.

We plot our $\Delta C/T_c$ in Fig. 2 as functions of T_c/T_P in both linear and log-log plots. We see that $\Delta C/T_c$ drops faster with decreasing T_c in the underdoped regime, i.e., in the mixed phase. This behavior is consistent with experimental data. The T dependence of $\Delta C/T_c$ is not exactly T^2, but looks reasonably close to T^2 in log-log plot (right panel in Fig. 2), although such a plot puts more weight on the data at low T_c where the T dependence of $\Delta C/T_c$ is the strongest.

Finally, we note that $\Delta C/T_c$ is discontinuous at the tetra-critical point $T_c = T_s = T_P$. The discontinuity is the manifestation of the discontinuous change in both α' and β across T_P. The discontinuity in α' is due to the fact that the second term in Eq. (27) is zero for $M = 0$, but is finite when $M \neq 0$ and contains temperature derivative of $(g^{(0)}_{\omega_n} - 1) \propto M^2 \propto (T - T_P)$. The discontinuity in β is due to the feedback term C^2/B in β, which remains finite upon approaching T_P from smaller dopings, but is absent in the overdoped regime, where $T_s < T_c$. The interplay between discontinuities in α' and β in the disorder model is such that $\Delta C/T_c$ jumps up at $n_{\rm imp}$ once the system enters the mixed phase.

The discontinuity in $\Delta C/T_c$ at T_P has also been found in the rigid-band model.[19] In that model, however, the magnitude and the sign of the jump in $\Delta C/T_c$ depend on the FS geometry and $\Delta C/T_c$ may actually drop down upon entering into the mixed phase. We also emphasize that discontinuity in $\Delta C/T_c$ only holds within the mean-field theory and gets rounded up and transforms into a maximum once we include fluctuations because then the thermodynamic average $\langle M^2 \rangle$ is nonzero on both sides of the tetra-critical point. This behavior of $\Delta C/T_c$ in the presence of fluctuations is schematically illustrated in Fig. 1(b) by the dashed line.

VI. CONCLUSIONS

In this paper, we obtained the phase diagram of doped Fe-pnictides and the specific heat jump ΔC at the onset of superconductivity across the phase diagram under the assumption that doping introduces disorder but does not affect the band structure. The phase diagram is quite similar to the one obtained in the rigid band scenario and contains SDW and SC phases and the region where SDW and SC orders coexist. The ratio $\Delta C/T_c$, which is a constant in a BCS superconductor, is nonmonotonic across the phase diagram—it has a maximum at the tetra-critical point at the onset of the mixed phase and drops at both larger and smaller dopings. The behavior at large and small dopings is described in terms of the single parameter: the impurity density $n_{\rm imp}$. The nonmonotonic behavior of $\Delta C/T_c$ in the underdoped regime also holds in the rigid band model,[19] but there the behavior of $\Delta C/T_c$ at small and large dopings is generally uncorrelated.

We found reasonably good agreement between our theory and the experimental phase diagram of $Ba(Fe_{1-x}Ru_x)_2As_2$ in which Fe is subsituted by isovalent Ru (see Refs. 6 and 7) and on the data for the doping dependence of the specific heat jump at T_c (see Refs. 15–17). This agreement is a good indicator that our theory captures the key physics of nonmonotonic behavior of $\Delta C/T_c$, particularly the reduction of $\Delta C/T_c$ in the mixed state. Whether the data can distinguish between rigid-band and disorder scenarios is a more subtle issue as the interplay between doping-induced disorder and doping-induced change in the band structure is likely to be material dependent. Another subtle issue is the apparent T^2 dependence of the measured $\Delta C/T_c$ on both sides of optimal doping. Our log-log plots reproduce this dependence reasonably well, but our actual $\Delta C/T_c$ are more mild than T^2. One possible reason is our neglect of the doping dependence of γ in the normal-state specific heat $C = \gamma T$. In reality, γ also decreases on both sides of optimal doping,[16] and this should sharpen up the T dependence of $\Delta C/T_c$.

Finally, there are certainly other elements of the physics of $Ba(Fe_{1-x}Ru_x)_2As_2$, which we neglected in our model. In particular, Brouet*et al.* demonstrated[6] that Fermi velocities in $Ba(Fe_{1-x}Ru_x)_2As_2$ are larger than in undoped $BaFe_2As_2$, this observation likely implies that electronic correlations are weaker in $Ba(Fe_{1-x}Ru_x)_2As_2$. Dhaka *et al.* argued[7] that magnetic dilution due to Ru substitution contributes to the destruction of SDW order. These effects add on top of Ru-induced impurity scattering, which we studied here, and call for more comprehensive analysis of isolvalent doping of Fe in 122 materials.

ACKNOWLEDGMENTS

We thank S. Budko, P. Canfield, R. Fernandes, F. Hardy, I. Eremin, A. Kaminski, N. Ni, J. Schmalian, and A. Vorontsov for useful discussions. M.G.V. and A.V.C. are supported by NSF-DMR 0955500 and 0906953, respectively.

[1] P. Hirschfeld, M. Korshunov, and I. Mazin, Rep. Prog. Phys. **74**, 124508 (2011).
[2] H. Wadati, I. Elfimov, and G. A. Sawatzky, Phys. Rev. Lett. **105**, 157004 (2010).
[3] R. M. Fernandes *et al.*, Phys. Rev. B **81**, 140501 (2010).
[4] A. B. Vorontsov, M. G. Vavilov, and A. V. Chubukov, Phys. Rev. B **79**, 060508 (2009).
[5] V. Cvetkovic and Z. Tesanovic, Europhys. Lett. **85**, 37002 (2009).
[6] V. Brouet *et al.*, Phys. Rev. Lett. **105**, 087001 (2010).
[7] R. S. Dhaka *et al.* (2011), e-print arXiv:1108.0711 (unpublished).
[8] A. Kaminski (private communication).
[9] C. Tarantini *et al.*, Phys. Rev. Lett. **104**, 087002 (2010).
[10] H. Kim *et al.*, Phys. Rev. B **82**, 060518 (2010).
[11] N. I. Kulikov and V. V. Tugushev, Usp. Fiz. Nauk **144**, 643 (1984) [Sov. Phys. Usp. **27**, 954 (1984)].
[12] O. V. Dolgov, A. A. Golubov, and D. Parker, New J. Phys. **11**, 075012 (2009).
[13] A. B. Vorontsov, M. G. Vavilov, and A. V. Chubukov, Phys. Rev. B **79**, 140507 (2009).
[14] Y. Bang, Europhys. Lett. **86**, 47001 (2009).
[15] S. L. Bud'ko, N. Ni, and P. C. Canfield, Phys. Rev. B **79**, 220516 (2009).
[16] F. Hardy, T. Wolf, R. A. Fisher, R. Eder, P. Schweiss, P. Adelmann, H. v. Löhneysen, and C. Meingast, Phys. Rev. B **81**, 060501 (2010).
[17] F. Hardy *et al.*, Europhys. Lett. **91**, 47008 (2010).
[18] Z.-S. Wang, H.-Q. Luo, C. Ren, and H.-H. Wen, Phys. Rev. B **78**, 140501 (2008).
[19] M. G. Vavilov, A. V. Chubukov, and A. B. Vorontsov, Phys. Rev. B **84**, 140502(R) (2011).
[20] A. V. Chubukov, D. V. Efremov, and I. Eremin, Phys. Rev. B **78**, 134512 (2008).

[21] S. Maiti and A. V. Chubukov, Phys. Rev. B **82**, 214515 (2010).
[22] F. Wang, H. Zhai, Y. Ran, A. Vishwanath, and D.-H. Lee, Phys. Rev. Lett. **102**, 047005 (2009).
[23] R. Thomale, C. Platt, J. Hu, C. Honerkamp, and B. A. Bernevig, Phys. Rev. B **80**, 180505 (2009).
[24] C. Platt, C. Honerkamp, and W. Hanke, New J. Phys. **11**, 055058 (2009).
[25] G. Eilenberger, Z. Phys. **214**, 195 (1968).
[26] A. Moor, A. F. Volkov, and K. B. Efetov, Phys. Rev. B **83**, 134524 (2011).
[27] A. A. Abrikosov and L. P. Gor'kov, ZhETF **39**, 1781 (1960) [Sov. Phys. JETP **12**, 1243 (1961)].
[28] A. V. Balatsky, I. Vekhter, and J.-X. Zhu, Rev. Mod. Phys. **78**, 373 (2006).
[29] V. Galitski, Phys. Rev. B **77**, 100502 (2008).
[30] A. B. Vorontsov, A. Abanov, M. G. Vavilov, and A. V. Chubukov, Phys. Rev. B **81**, 012508 (2010).
[31] E. G. Moon and S. Sachdev, Phys. Rev. B **82**, 104516 (2010).
[32] A. A. Abrikosov, L. P. Gorkov, and I. E. Dzyaloshinski, *Methods of Quantum Field Theory in Statistical Physics*, (Dover, New York, 1963); E. M. Lifshitz and L. P. Pitaevski, *Statistical Physics*, (Pergamon, 1980).
[33] V. G. Kogan, Phys. Rev. B **80**, 214532 (2009).